Superior Fischer-Tropsch performance of uniform cobalt nanoparticles deposited into mesoporous SiC

V. Iablokov[a,b], S.A. Alekseev[c,d], S. Gryn[c,d], I. Bezverkhyy[e], V. Zaitsev[f], L. Kovarik[g], T. Visart de Bocarme[b], N. Kruse[a,h]

[a] *Voiland School of Chemical Engineering and Bioengineering, 1505 NE Stadium Way, Washington State University, Pullman, WA 99164, United States*

[b] *Université Libre de Bruxelles, Chemical Physics of Materials, Campus Plaine, CP243 Brussels, B-1050, Belgium*

[c] *Taras Shevchenko National University of Kyiv, 64, Volodymyrska Street, 01601 Kyiv, Ukraine*

[d] *Science Park Kyiv Taras Shevchenko University, 60, Volodymyrska Street, 01033 Kyiv, Ukraine*

[e] *Laboratoire Interdisciplinaire Carnot de Bourgogne, UMR CNRS 6303, Universite de Bourgogne, Dijon, France*

[f] *Chemistry Department, Pontifical Catholic University of Rio de Janeiro, Rua Marques de Sao Vicente, 225-Gavea, Rio de Janeiro 22451-900, Brazil*

[g] *Environmental Molecular Sciences Laboratory, Pacific Northwest National Laboratory, P.O. Box 999, Richland, U.S.A.*

[h] *Institute for Integrated Catalysis, Pacific Northwest national Laboratory, Richland, WA 99332, U. S.A.*

Abstract

Electrochemically-derived well-crystalline mesoporous silicon carbide (pSiC) was used as a host for cobalt nanoparticles to demonstrate superior catalytic performance during the CO hydrogenation according to Fischer-Tropsch. Colloidal Co nanoparticles (9 ± 0.4 nm) were prepared independently using colloidal recipies before incorporating them into pSiC and, for comparison purposes, into commercially available silica (Davisil) as well as foam-like MCF-17 supports. The Co/pSiC catalyst demonstrated the highest (per unit mass) catalytic activity of 117 $\mu mol_{CO}\ g_{Co}^{-1}\ s^{-1}$ at 220 °C which was larger by about one order of magnitude as compared to both silica supported cobalt catalysts. Furthermore, a significantly

higher C_{5+} hydrocarbons selectivity was observed for Co/pSiC. The stable performance of the catalyst is attributed to the high dispersion of the active phase and the use of pSiC acting as a thermally conductive and chemically inert mesoporous support.

Keywords: mesoporous silicon carbide, MCF-17, cobalt nanoparticles, Fischer-Tropsch, CO hydrogenation

1. Introduction

The search for alternative energy sources is a strategic task for the immediate future. Renewable biomass, large deposits of natural gas and, less preferably, coal can be such sources. Technologically, syngas, a gas mixture of CO and H_2, is being used for fuel and chemical feedstock production according to Fischer-Tropsch (FT) [1]. The FT process usually employs Fe and Co-based catalysts supported on silica or alumina with the main focus on synthesizing naphtha, transport fuels, kerosene and lubricant oils [2, 3]. Recent studies have also demonstrated the production of long chain terminal alcohols, aldehydes and/or short chain olefins with high selectivity from syngas as, for example, described in ref. [4-7].

One of the main technological challenges in large-scale applications of the Fischer-Tropsch process is associated with the temperature control due to the high exothermicity of the reaction [8-10]. Metal sintering may be incurred by insufficient heat dissipation and is generally accepted to be the main reason for catalysts deactivation [8,9]. In particular, the use of poorly thermo-conductive supports, such as silica or alumina, may cause local overheating in the catalyst. However, other deactivation mechanisms involving carbon deposition and side reactions with the support, further promoted by H_2O (which always accompanies hydrocarbon formation), may be encountered at high conversion rates. In general, the addition of noble metals may provide a remedy. Ru, Re and Pt were shown to facilitate the reduction of cobalt oxide and to improve Co metal dispersion [2, 11, 12]. A similar stabilization effect was reported for cobalt-based catalysts promoted with ZrO_2 [13]. On the other hand, Jacobs et al. [9] reported that noble metals may also cause a faster deactivation due to the formation of unstable cobalt (0) clusters on the surface of the catalysts. These clusters turned out to be prone to sintering and reoxidation.

Quite different from stability considerations, promotion with metal oxides containing, for example, Mn, La and others, primarily aims at optimizing the activity and selectivity of FT catalysts [3]. Water product causes hydrothermal conditions which may lead to oxidation of the active phase and continuous disruption of the support. Such damage is one of the major drawbacks in the use of well-defined mesoporous silica materials [14-16]. Under these conditions, the chemical and physical nature of the

support material plays a crucial role. To find a remedy, several reports mention the use of carbon-based materials [17-19] which, however, undergo oxidation to CO_2 during regeneration in air and also present considerable health concerns when handling them.

The search for process-adapted solutions has brought scientists to explore porous silicon carbide as a potential catalyst support candidate for temperature-sensitive catalytic reactions. Silicon carbide (SiC) is known for its high thermal conductivity (120 W m^{-1} K^{-1} for 3C-SiC as compared to 1.4 W m^{-1} K^{-1} for SiO_2), inertness and mechanical stability [20]. A series of studies over Co-supported catalysts were reported using commercially available porous silicon carbide supplied by SiCAT company [21]. The selectivity to C_{5+} hydrocarbons reached more than 90% at high CO conversion (>50%) [22-27] which is clearly superior to catalysts using silica or alumina as support. The authors related the improved C_{5+} selectivity to the efficient heat release and weaker metal-support interaction compared to catalysts using silica supports. However, the activity on a per mass basis for β-SiC was considerably lower than for standard alumina/silica in Co-based catalysts [28]. This loss in activity may be related to the ill-defined pore framework and insufficient pore volume when impregnating the active phase. The reported BET surface area of the silicon carbide supplied by SiCAT was about several tens of m^2 g^{-1}, with the pore volume being below 0.15 cm^3 g^{-1}. Furthermore, commercial porous SiC contains admixtures, such as carbon, silicon oxocarbide, amorphous or highly-defective SiC, and may include impurities acting as inhibitors [27].

In the present work, we use mesoporous silicon carbide prepared by electrochemical etching [29] before depositing uniform cobalt nanoparticles for studies of the Fischer-Tropsch process. The as-synthesized pSiC support demonstrates tunable textural parameters while retaining its high initial crystallinity [29]. The SiC's effective thermal conductivity and its chemical inertness may dissipate local overheating and therefore inhibit sintering of metal particles. Moreover, we anticipate methods of colloidal chemistry to be most valuable for obtaining uniform-in-size Co particles [30], subsequently loading them into the porous SiC host. Such colloidal particles preserve their initial size and can be efficiently distributed through the support under ultrasonic treatment. Previously, we successfully used this approach to prepare model Co/MCF-17 and Fe(0)/MCF-17 catalysts for CO_2 and CO hydrogenation studies, respectively [6, 30].

2. Materials and Methods

2.1. Porous SiC preparation by electrochemical etching

The anodic etching of bulk 3C-SiC polycrystalline wafer (n-type, resistivity 0.7 mΩ cm, thickness 4 mm) was performed in a Teflon cell with a copper electrode as a backside contact and a gold counter-electrode. Applied conditions include: no mixing, 60 cm^2 etched area, current density j= 50 mA cm^{-2}, etching time t= 6 h, HF aqueous solution (13 wt%) as electrolyte. After etching, a light-brown layer on top of the SiC plate was rinsed off with deionized water, dried and collected by mechanical scratching, providing approx. 1 g of powder. Before characterization and Co NPs intercalation, the porous SiC samples were annealed at 500 °C for 1 h in air to remove the carbon-enriched surface layer and any traces of carbon fluorooxide [31, 32]. More detailed information can be found in ref. [29].

2.2. Synthesis of Co nanoparticles

Dicobalt octacarbonyl was supplied by Strem; o-dichlorobenzene (99%, anhydrous), oleic acid (90%, technical grade), and all solvents were purchased from Sigma-Aldrich Company. Monodisperse metallic cobalt nanoparticles were synthesized by swift injection of 0.52 g of cobalt carbonyl precursor in 3 mL of dichlorobenzene (DCB) to the refluxing solution of 12 mL DCB and 0.15 mL oleic acid at 174 °C [30]. After 15-20 min refluxing, the synthesis was stopped by addition of 10 mL DCB to decrease the temperature. The colloids were precipitated in 140 mL of 2-propanol and centrifuged at 4000 rpm for 5 min, followed by redispersion in a small volume (1-2 mL) of hexane. Then, the washing step was repeated using an ethanol/methanol (3:1 by volume) solution to precipitate the colloids; subsequent centrifugation and redispersion in 30 mL of chloroform led to the colloidal solution of uniform-in-size cobalt particles of 9 ± 0.4 nm. We found it critically important that cobalt particles were washed twice using a methanol/ethanol (1:3) solution this time. Such treatment provides reliable and reproducible results in the catalytic studies.

2.3. Preparation of supported catalysts

Cobalt nanoparticles were incorporated into porous silicon carbide (pSiC), commercially available silica Davisil Grade 643 (Dav) supplied by Sigma Aldrich, and meso-cellular silica foam (MCF-17, denoted as MCF). The MCF-17 was prepared according to the protocol described in [33]. All supports were calcined in air at 350 °C prior to impregnation. Typically, 0.40 - 0.45 g of powders were wetted with 5-7 mL of chloroform. 5 mL of the as-prepared cobalt NPs dispersed in chloroform were added and sonicated for 1 h; subsequent centrifugation at low speed (1000 rpm) allowed separation of the samples from cobalt NPs residing in the solution. The samples were dried in vacuum at 100 °C for 1 h. AAS was applied to determine cobalt loading. The obtained samples were denoted as Co/pSiC, Co/MCF and Co/Dav, and the respective cobalt loadings were 4.74%, 2.78% and 1.01% in order of mention. The samples were subsequently reduced in 85% hydrogen (Ar as balance) using temperature-programmed reduction (TPR)

at a total flow rate of 30 cm^3 min^{-1}. The reduction was performed at 460 °C (heating rate of 10 °C min^{-1}) for 2 h in an U-type reactor. For comparison, a non-supported cobalt sample (bulk Co) was synthesized through oxalate precipitation followed by activation in hydrogen flow at 420 °C. Unlike oriented Co single crystals, such Co bulk provides an appropriate texture with low yet sufficient specific surface area for high-pressure catalytic tests, as reported, for example, in ref. [4].

2.4. Measurements and characterization

Nitrogen adsorption/desorption isotherms were measured using a Micromeritics ASAP 2020 system at 77 K. Powder X-ray diffraction (XRD) patterns were collected on a D8 Advance Bruker diffractometer equipped with a CuKα X-ray source. TEM images were taken on a JEOL JEM 2100 high resolution transmission electron microscope with an accelerating voltage of 200 kV. Scanning transmission electron microscopy (STEM) images were collected in high angle annular dark field (HAADF) mode using a probe-corrected Titan 80−300 TEM operated at 300 kV.

Temperature programmed reduction and H_2-D_2 exchange measurements for metallic surface area determination were performed in a home-built flow system operated at ambient pressure. Samples were loaded into a well-mixed plug-flow U-type quartz reactor. A quadrupole mass spectrometer (Balzers QMG 422) was connected to the reactor via a capillary allowing the outlet flow to be continuously followed. In a typical experiment, a flow of deuterium (in argon) was set to 30 cm^3 min^{-1}. The temperature of the reactor was kept at 200 °C. Then, the feed was abruptly switched from D_2 to H_2 which led to the immediate formation of HD. The procedure was repeated using different partial pressures of D_2 and H_2. To exclude any influence by gas phase H_2-D_2 exchange in the reactor, a linear graph for the amount of formed HD was plotted against the partial pressure of hydrogen and extrapolated to zero pressure. The obtained number of HD molecules represented the number of adsorbed deuterium atoms on the metal surface before switching to H_2. A detailed description of the H_2/D_2 exchange method can be found elsewhere [30, 34].

2.5. Catalytic studies

High-pressure catalytic tests were performed in a fixed-bed plug-flow reactor consisting of a quartz tubule (d_{inner}= 5 mm) inserted into a stainless steel housing. Typically, 0.25 – 0.4 g of a catalyst sample were loaded in the isothermal region of the reactor, and then activated in-situ with H_2 at 1 bar (40 cm^3 min^{-1}) up to 460 °C for 2 h. No bulk SiC was added to the catalysts except for studies with bulk Co (derived from cobalt oxalate as micrometer-sized aggregates with insufficient heat dissipation even in the presence of SiC). The reactor was subsequently cooled to 120 °C, and then CO was added to produce a 2:1 H_2/CO syngas feed with a total flow of 40 cm^3 min^{-1} (GHSV is 2000 h^{-1}). The total pressure was

subsequently raised to 20 bar. The synthesis temperature was approached using a low heating rate of 1.5 °C min^{-1}. The catalytic behavior was first measured at 240 °C (Run 1), then the temperature was allowed to decrease to 220 °C (Run 2) followed by another increase to 240 °C (Run 3). Catalytic activities and product selectivities were determined after stabilization for at least 12 h for a given temperature using chromatography-mass spectrometry equipped with two sampling loops (GC-MS, Agilent 7890A-5975). The GC/MS system was connected through the capillary in the outlet of the high pressure reactor. The capillary was wrapped with heating tape and kept at 200 °C to avoid condensation of heavy hydrocarbons. Two connected columns in backflush mode (3 Foot and 9 Foot Hayesep Q 80/100) were used to analyze light gases (up to C_3) in the TCD detector, while the DB-1 capillary column determined C_{4+} hydrocarbons and alcohols eluted to the MS detector. The CO conversion was determined by summing up all the carbon products and considering the carbon balance (including CO). The GC/MS system allows determining the entire spectrum of products (light gases and heavy fraction) simultaneously at any given point in time without using separators (hot and cold traps). Note that the use of separators flattens the product yield and conceals deactivation patterns. Our GC/MS system allows determination of hydrocarbons up to dodecane.

Metal dispersion D (%) and TOF values (s^{-1}) based on H_2-D_2 exchange measurements were calculated by assuming hydrogen adsorption on cobalt at 200 °C to occur dissociatively with a stoichiometry of 1 H atom per metallic Co surface atom as follows:

$D = n_{HD} * 59$, and $TOF = \frac{R}{n_{HD}}$

where n_{HD} is the number of HD moles per gram of cobalt particles ($mol_{HD}\ g_{Co}^{-1}$).

3. Results and discussions

3.1. Properties of the SiC support

In our recent work [29], we provided a detailed characterization of porous SiC as obtained from the electrochemical etching of SiC polycrystalline wafers. For the present catalytic studies, we made use of the favorable textural and morphological characteristics of porous SiC (pSiC) which qualify it as an excellent support material.

Quite generally, the slightly yellowish-white color of the pSiC powder after thermal oxidation at 500 °C already indicates the absence of a significant fraction of admixtures such as amorphous carbon and/or amorphized SiC_{1+x} phase, which are usually dark-colored. Nitrogen physisorption isotherms of the pSiC sample (Figure 1a) show type IV behavior, with a narrow H3 type hysteresis loop indicating the presence

of slip-shaped mesopores. The textural parameters derived from the isotherm (120 m^2 g^{-1} surface area, 0.70 cm^3 g^{-1} pore volume) and the BJH pore size distributions with maxima at 23 nm (adsorption) and 18 nm (desorption), allow us to classify pSiC as a mesoporous material with an open pore framework.

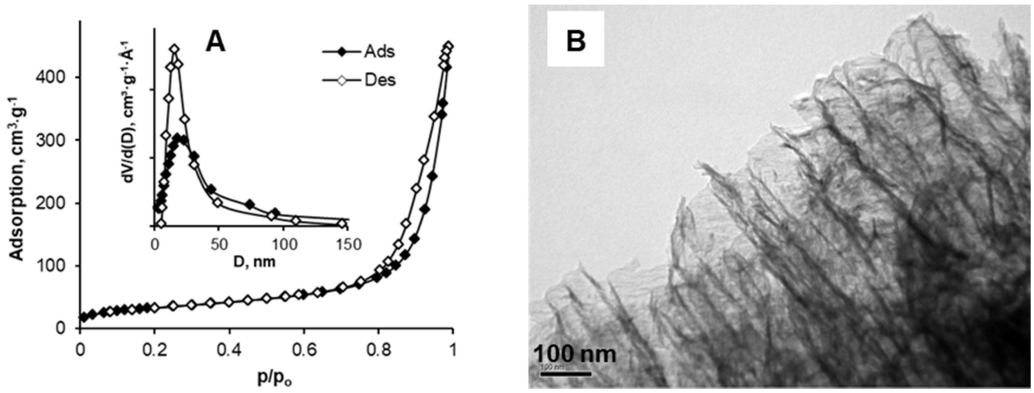

Figure 1. Characterization data of electrochemically-derived porous SiC: a) Nitrogen adsorption/desorption isotherms and BJH pore size distributions (inset), and b) TEM image (scale bar is 100 nm)

TEM analysis (Figure 1b) revealed a dendritic morphology composed of 10-15 nm thick SiC wire-like crystallites and about 20 nm inter-crystallite pores, which correlates well with the N_2 isotherm data. Quite evidently, such open interconnected mesoporous morphology would appear to be perfectly suited for hosting Co NPs (9 nm in our case) in catalytic applications.

3.2. Activation of Co-supported samples

Colloids of uniform cobalt nanoparticles were intercalated under ultrasonic conditions into porous SiC and silica foam-like MCF-17. TEM images of the resulting samples are shown in Figure 2 along with virgin Co NPs. Due to the thickness of the supports' structure, metal particles become only visible in the periphery of the pore frameworks.

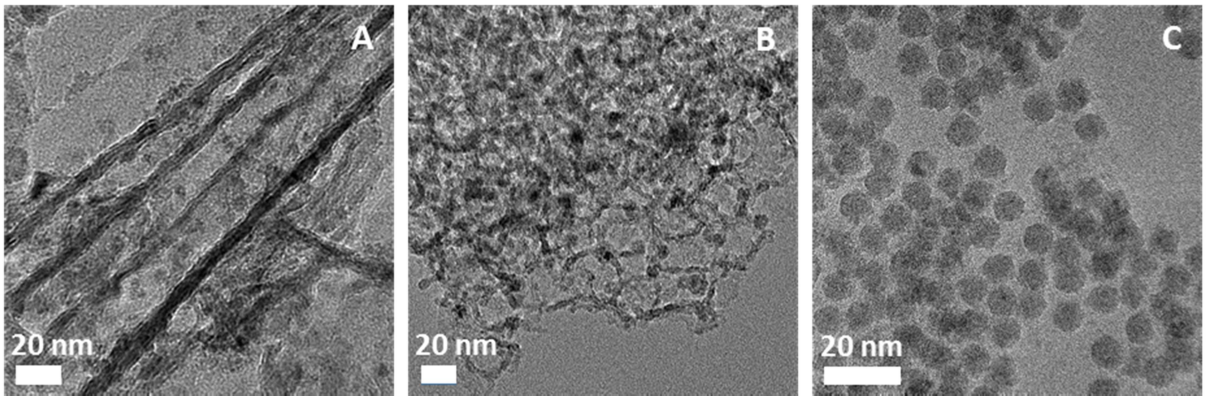

Figure 2. TEM images of Co nanoparticles intercalated into a) porous SiC, b) MCF-17, and c) colloid of virgin Co NPs

The porous SiC and MCF-17 materials demonstrate well-defined 3D pore structure that can be distinguished in TEM images as accessible 'trunks' in pSiC, and rigid walls of cell-like pores in MCF-17, respectively. On the other hand, preparations with Davisil silica are characterized by ill-defined porosity, with insufficient contrast to reveal metallic particles in TEM (see SI, Figure S1). Bulk cobalt prepared via oxalate precipitation, a method frequently used in our laboratory, is composed of irregular aggregates of the metal. Due to the absence of a support material (Figure S1) its surface area is lower (1.1 $m^2 g^{-1}$) than that of all other samples. The textural parameters are summarized in Table 1. It should be noted, that we also used commercially available porous β-SiC to host colloidal Co nanoparticles. However, the textural characteristics did not provide sufficient pore volume and/or anchor sites for an optimal cobalt weight loading; catalytic studies therefore led to low CO conversion (<0.2%).

Table 1. Textural properties of support materials

Sample	S ($m^2 g^{-1}$)	V_{pore} ($cm^3 g^{-1}$)	Pore size (nm)*
Porous SiC (pSiC)	120	0.70	18
MCF-17 (MCF)	492	2.2	10.1
Davisil Grade 643 (Dav)	223	1.2	10.7
Cobalt bulk	1.1	-	-
β-SiC (SiCAT)	23.1	0.12	14.8

* Average pore size from BJH pore size distribution

Prior to catalytic studies, all samples were subjected to a flow of hydrogen while heating them in a temperature-programmed manner at a rate of 10 °C/min. This caused metal reduction and removal of

oleic acid present as capping surfactant in colloidal Co sample preparations. As an example, Figure 3 shows the mass spectrometric evolution of m/z=15 during TPR for the Co/pSiC sample.

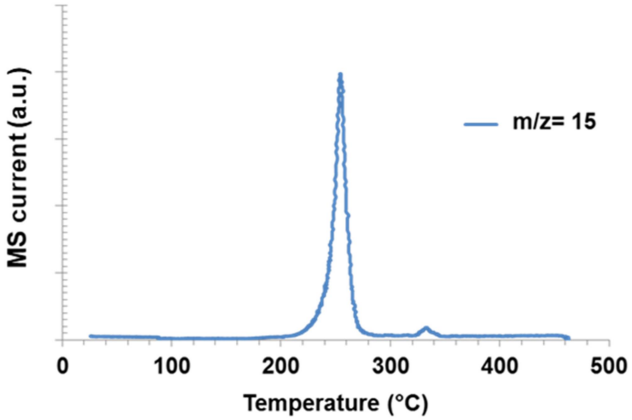

Figure 3. TPR profile of Co/pSiC sample treated in 85% H_2/Ar flow up to 460 °C

The m/z=15 peak is characteristic for methane formation and was always observed to occur at 255 °C for all the supports. Note that methane is the dominating product during hydrogenolysis of long-chain oleic acid.

3.3 Catalytic results

Catalytic studies were carried out at 220 °C and 240 °C while keeping the pressure constant at 20 bar and adjusting a partial pressure ratio of p_{H2}/p_{CO}=2. The catalytic performance in terms of activity and products selectivity is summarized in Figure 4 and Table 2.

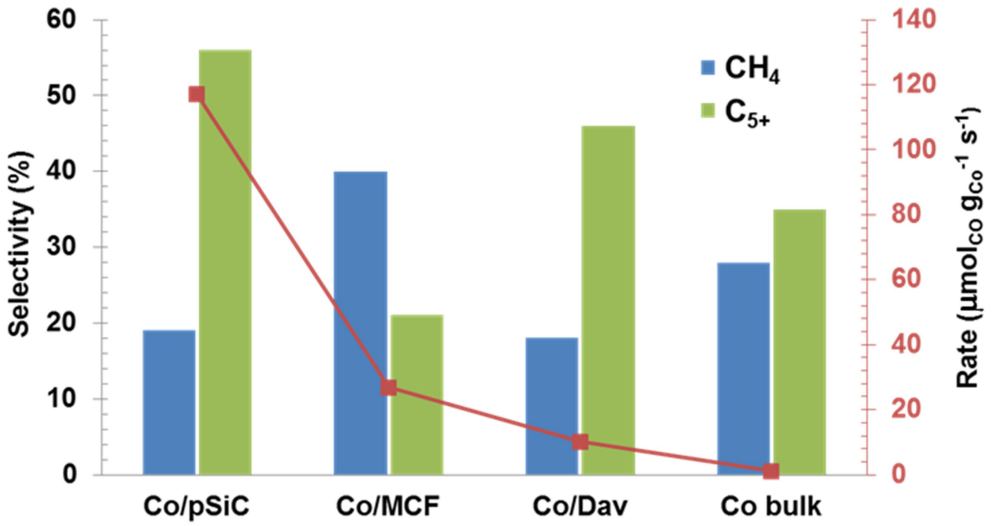

Figure 4. Activity and selectivity of catalysts in the Fischer-Tropsch process (Reaction conditions: 220 °C, 20 bar, H_2:CO = 2:1, total flow is 40 cm^3 min^{-1})

As can be seen from this figure, the Co/pSiC sample provides a superior reaction rate among the various catalysts; a rate of 117 μmol_{CO} g_{Co}^{-1} s^{-1} is obtained which is possibly the highest, or at least one of the highest, ever reported. Literature data mention a range of 10-50 μmol_{CO} g_{Co}^{-1} s^{-1} for active Co-based catalysts under similar conditions [3, 35]. According to figure 4, both, Co particles supported on MCF-17 and Davisil silica (Co-Dav) fall into this range, with rates of 28.8 and 10.2 μmol_{CO} g_{Co}^{-1} s^{-1}, respectively. A significant difference is also observed with respect to the CO conversion. Co/pSiC shows a considerably higher CO conversion of 28.2% as compared to the other supports (below 2%). Unfortunately, such large difference in the activity (much larger than anticipated with regard to nominal Co loadings) may bias the selectivity patterns [36, 37], as discussed below. We note in this context that in the present research work we primarily focus on evaluating the stability performance using different supports, so high conversion is mainly contemplated here.

Table 2. Activity and selectivity of Co-based catalysts at 220 °C (pressure is 20 bar, H_2:CO = 2:1, total flow is 40 cm^3 min^{-1})

Sample	CO conv. (%)	Reaction rate (μmol_{CO} g_{Co}^{-1} s^{-1})	D (%)	TOF (s^{-1})	Selectivity (%)					α*
					CH_4	C_2-C_4	C_{5+}	ROH	CO_2	
Co/pSiC	28.2	117	8.4	0.082	19	18	56	5	2	0.80
Co/MCF	2.09	26.8	2.1	0.077	40	30	21	5	4	0.71

Co/Dav	0.52	10.2	0.9	0.065	18	18	45	7	12	0.81
Co bulk	0.91	1.0	-	0.039**	28	28	35	3	6	0.73

* α is the chain lengthening factor

**TOF value for Co bulk was calculated on the basis of the BET area for the passivated sample

TOF values in Table 2 show relatively little dependence of the support (disregarding data for bulk Co for which the specific surface areas are low and therefore afflicted with a relatively high degree of uncertainty). This is in agreement with literature reports, where no significant influence of the support material on the 'turnover frequency' was observed [2, 35, 38, 39]. Since the error in chemisorption measurements is relatively high (about 20% or even somewhat higher, depending on the assumptions made), the slight decrease for the Co/Dav sample (0.065 s^{-1}) as compared to Co/pSiC and Co/MCF (0.082 s^{-1} and 0.077 s^{-1}, respectively) is probably not significant. On the other hand, Table 2 confirms that the cobalt dispersion figures are highest for Co/pSiC. A numerical value of 8.4% corresponds to an average cobalt particle size of 11.4 nm while the corresponding figures for MCF (2.1%) and Dav (0.9%) samples lead to 47 nm and 104 nm, respectively. Thus, sintering effects appear particularly serious for Co/Dav which is in line with SEM studies, see Figure S2. Similar deactivation processes likely take place in Co/MCF-17, see Figure S3. Besides sintering, we relate the reduced activity to a continuous disruption of the silica pore framework.

Lacroix et al. [22] and Liu et al. [23] explored the possibilities of improving the activity over commercially available β-SiC support. For instance, decorating β-SiC with TiO_2 followed by its impregnation with a solution of Co-nitrate, led to the formation of smaller cobalt particles ranging between 5 and 15 nm as compared to 30-50 nm for Co on β-SiC [23]. However, such modification did not provide a noticeable increase in the activity: 53 $\mu mol_{CO}\ g_{Co}^{-1}\ s^{-1}$ versus 75 $\mu mol_{CO}\ g_{Co}^{-1}\ s^{-1}$ (at 230 °C, 40 bar) over 10Co/SiC and 10Co/TiO_2-SiC, respectively [23]. According to the authors' ^{59}Co NMR and TEM characterization studies, the major fraction of Co atoms (about 70%) appeared aggregated to a few very large-sized particles. The authors observed the broad particle size distribution of their samples to result in moderate activity. This is different from our case where the superior reaction rate (117 $\mu mol_{CO}\ g_{Co}^{-1}\ s^{-1}$) over the Co/pSiC has been achieved thanks to the high dispersion of the active phase.

As to the selectivity signatures, we observe that Co/pSiC performs best in C_{5+} production. According to Figure 4 and Table 2, a nearly 35% and 11% increase is obtained for the yield of long-chain hydrocarbons (C_{5+}) compared to Co/MCF and Co/Dav, respectively. Furthermore, the Co/MCF catalyst stands out for its high (unwanted) methane formation (40%). We suggest that the relatively thin walls of the silica pore framework in this catalyst get disrupted, possibly involving Co-silicate formation. Wei et al. [40], in their

studies of cobalt impregnated into MCF-like silica supports, reported a fast deactivation and loss in selectivity due to cobalt sintering and formation of Co-silicate compounds. A slight increase in the CO_2 formation is visible for the Co/Dav sample. Literature frequently associates CO_2 formation with the occurrence of the water gas shift reaction. On the other hand, according to mechanistic studies in our laboratory, CO_2 has to be regarded a signature species resulting from the occurrence of oxygen-containing (carboxyl-type) surface species [41]. It is not possible, at present, to relate the increased CO_2 formation over Co/Dav to either process. Bulk Co shows low activity according to Figure 4/Table 2, possibly due to the limited metal surface area (1.1 m^2 g^{-1} in BET measurements). The yield to C_{5+} hydrocarbons is also lower than that observed for the other catalysts tested here. As mentioned previously, the performance of bulk Co is negatively influenced by an insufficient removal of the heat of reaction. To allow a more detailed assessment of the chain-lengthening capacities of the various catalysts investigated here, Anderson-Schulz-Flory (ASF) distributions (excluding methane and ethane) are constructed and shown in Figure 5.

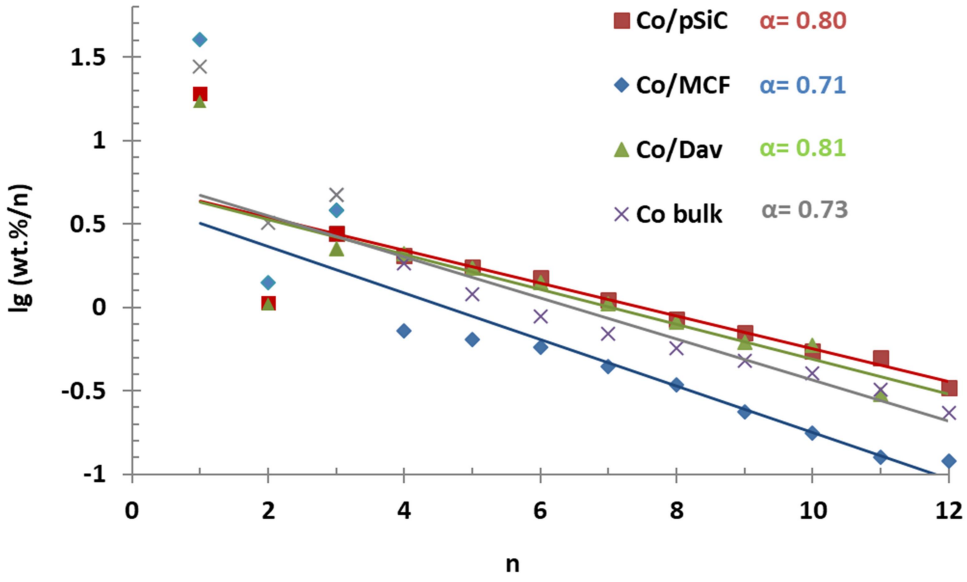

Figure 5. Product distribution according to ASF model (Reaction conditions: 220 °C, 20 bar, H_2:CO = 2:1, total flow is 40 cm^3 min^{-1})

Quite generally, all catalysts show a straight-line ASF dependence for C_{4+} hydrocarbons while major deviations are encountered for short-chain products. Such deviations are well-known and have been reported for decades of Fischer-Tropsch research. Chain-lengthening probabilities according to Figure 5

are between 0.71 and 0.81. All catalysts show a significant overshoot for methane production, which may have various reasons. Due to the colloidal preparation route chosen for the synthesis of Co nanoparticles and their anchoring in pSiC and Dav/MCF silica supports, carbon residues originating from the use of oleic acid as surfactant may be suspected to undergo hydrogenation to (mainly) methane, in agreement with the TPR results presented in Figure 3. The influence of residual carbon on the catalytic performance was previously also described by Cargnello et al. [42] and Park et al. [43]. Both groups reported ozone-UV treatment or fast pyrolysis to be efficient in carbon removal. The relatively high methane yields over bulk Co, prepared via Co-oxalate decomposition, are possibly due to local overheating and surface carbon formation. Quite interestingly, and not well understood at present [44, 45], the C_2 yields fall short for Co/pSiC and Co/Dav while they are close to "ASF expectations" for Co/MCF and bulk Co. Just the opposite behavior is observed for the C_3 yields: while they fit the straight-line dependence for Co/pSiC and Co/Dav, considerable "positive" deviations are encountered for Co/MCF and bulk Co.

We have also subjected all catalysts to longer-term performance tests in three successive runs starting at 240 °C, then 220 °C and back to 240 °C for 12 hours time-on-stream each. The data are compiled in Table 4.

Table 4. Stability patterns of Co-based catalysts (each temperature segment was kept for 12 h)

Sample	Run 1 at 240 °C			Run 2 at 220 °C			Run 3 at 240 °C		
	CO conv. (%)	Selectivity (%)		CO conv. (%)	Selectivity (%)		CO conv. (%)	Selectivity (%)	
		CH_4	C_{5+}		CH_4	C_{5+}		CH_4	C_{5+}
Co/pSiC	42.1	28	42	28.2	19	56	43.3	22	45
Co/MCF	8.9	30	35	2.1	40	21	7.0	43	21
Co/Dav	1.8	18	44	0.5	18	45	2.0	17	46
Co bulk	4.4	25	37	0.9	28	34	2.9	53	19

Accordingly, the Co/pSiC sample fully retains its initial CO conversion at 240 °C while methane and C_{5+} selectivities seem to be reduced and increased, respectively. Quite differently, Co/MCF and Co bulk samples show a noticeable deterioration in terms of activity and C_{5+} production. Co/Dav demonstrates low but stable conversion while the selectivity signature remains largely unchanged.

Finally, we have also carried out some further stability/characterisation studies for Co/pSiC and Co/Dav at higher temperature in an ambient pressure reactor. We find that after high-temperature CO hydrogenation at 300-340 °C (p_{H2}/p_{CO}=2, total pressure 1 bar), the Co/Dav sample loses its original activity while the Co/pSiC sample demonstrates stable behavior. Chemisorption experiments using H_2-D_2 exchange confirm that the metallic surface area of Co/pSiC remains unchanged during high temperature

catalytic tests. This is not the case for Co/Dav, see Table S1 and Figure S4. Since the activity loss actually turns out to be proportional to the decrease in chemisorption (metallic sites), we relate this observation primarily to the sintering and/or reaction of cobalt metal with the silica support at 340 °C, neglecting the possible occurrence of the Boudouard reaction in a first approximation.

3.4 STEM characterization

To gain more insight into possible FT reaction-induced changes of cobalt particles, the Co/pSiC sample has been subjected to a STEM analysis before and after catalytic testing.

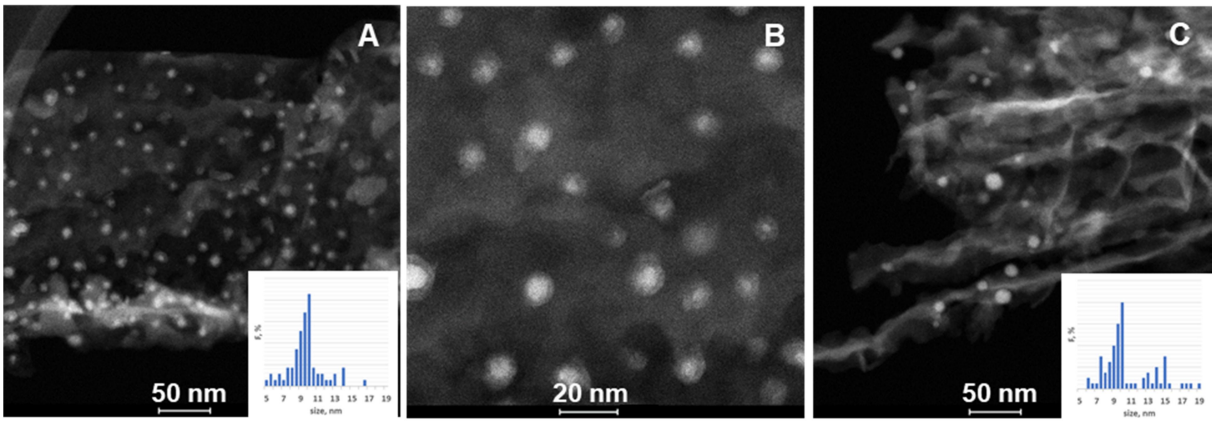

Figure 6. STEM images of cobalt particles intercalated into porous SiC: a, b) after TPR treatment, and c) after high-pressure FT reaction at conditions as defined in Figure 5

After catalyst activation and passivation (for STEM), cobalt particles are uniformly distributed over the support and appear in a core-shell structure due to the formation of a thin surface layer of cobalt oxide (Figure 6a, b). Hence, a particle size increase from initially 9 nm to 10 nm is observed. A rather limited broadening of the particle size distribution is found after catalytic testing. While a small fraction of the sintered particles appears with sizes in the range of 13-16 nm, the dominating part of cobalt particles retains its initial size centered at 9-10 nm (Figure 6c).

There seems to be little doubt that nanosized Co particles in mesoporous SiC are remarkably stable as compared to catalysts prepared according to traditional impregnation recipes, where the influence of metal precursor salts, chemical nature and texture of the support, drying and calcination conditions, to mention a few parameters, usually leads to particles with a broad distribution [46-48]. During catalysis, smaller particles may suffer continuous sintering through particle migration or Ostwald ripening. For instance, CO hydrogenation studies (H_2/CO= 2/1, 230 °C, 20 bar) on planar model catalysts [49, 50] showed that small cobalt particles below 5 nm disappeared while larger particles above 7 nm did not change their size. Furthermore, some larger particles merged when located close to each other. Tuning

the inter-particle distance for cobalt-based catalysts can also help control the activity in the Fischer-Tropsch process, as reported in ref. [51]. With regard to the use of SiC as a support, it is also worth mentioning that the formation of the active cobalt phase was observed to be strongly affected by the very nature of the β-SiC material, despite highly similar manufacturer specifications [52]. Different from impregnation methods, colloidal cobalt particle precursors are uniform in size and rather remote from each other after deposition into the mesoporous SiC structure (Figure 6a). Such uniform distribution of the active phase ensures an improved stability towards sintering. Moreover, the open structure of pSiC provides both high surface area and pore volume to host these particles. This stabilization effect, though not yet ideal, is rather unique when using pSiC as a support for Co nanoparticles.

In conclusion, the synergistic approach of using structurally well-defined mesoporous SiC hosting size-controlled Co nanoparticles has led to superior catalytic activity (per mass unit of the catalyst), and improved selectivity and stability in the Fischer-Tropsch process to C_{5+} hydrocarbons. The uniform size (9 ± 0.4 nm) of cobalt nanoparticles ensures high metal dispersion while mesoporous silicon carbide provides the necessary anchoring sites for metal particles and allows reactants to access and products to escape the inner parts of the pore network. The heat of reaction is efficiently dissipated thanks to the well-crystalline SiC structure. Our approach may help design new catalysts stable at high reaction rates under harsh reaction conditions (such as hydrothermal clause, high acidity, exothermic processes, oxidative regeneration steps, elevated temperatures, etc.) showing improved selectivity to desired product slates.

Acknowledgments

This work was supported by EU FP-7 Marie Curie Actions IRSES grant (GA 319013, “Porous Silicon Carbide as a Support for Co Metal Nanoparticles in Fischer-Tropsch Synthesis”) and EU Horizon 2020 MSCA-RISE (GA 690945, “Carbon-based nano-materials for theranostic application”), which are gratefully acknowledged. TEM part of this work was performed at the William R. Wiley Environmental Molecular Sciences Laboratory (EMSL) sponsored by the US Department of Energy, Office of Biological and Environmental Research located at Pacific Northwest National Laboratory (PNNL) under science theme proposal 49398.

References

[1] F. Fischer, H. Tropsch, Brennstoff-Chemie 4 (1923) 276.

[2] E. Iglesia, Appl. Catal., A 161 (1997) 59. https://doi.org/10.1016/S0926-860X(97)00186-5

[3] A.Y. Khodakov, W. Chu, P. Fongarland, Chem. Rev. 107 (2007) 1692. https://doi.org/10.1021/cr050972v

[4] Y. Xiang, N. Kruse, Nat. Commun. 7 (2016) 13058. https://doi.org/10.1038/ncomms13058

[5] H.M. Torres Galvis, J.H. Bitter, T. Davidian, M. Ruitenbeek, A.I. Dugulan, K.P. de Jong, J. Am. Chem. Soc. 134 (2012) 16207. https://doi.org/10.1021/ja304958u

[6] V. Iablokov, Y.Z. Xiang, A. Meffre, P.F. Fazzini, B. Chaudret, N. Kruse, ACS Catal. 6 (2016) 2496. https://doi.org/10.1021/acscatal.6b00346

[7] Y. Xiang, L. Kovarik, N. Kruse, Nat. Commun. 10 (2019) 3953. https://doi.org/10.1038/s41467-019-11836-z

[8] N.E. Tsakoumis, M. Rønning, Ø. Borg, E. Rytter, A. Holmen, Catal. Today 154 (2010) 162. https://doi.org/10.1016/j.cattod.2010.02.077

[9] A.M. Saib, D.J. Moodley, I.M. Ciobica, M.M. Hauman, B.H. Sigwebela, C.J. Weststrate, J.W. Niemantsverdriet, J. van de Loosdrecht, Catal. Today 154 (2010) 271. https://doi.org/10.1016/j.cattod.2010.02.008

[10] G. Jacobs, P.M. Patterson, Y. Zhang, T. Das, J. Li, B.H. Davis, Appl. Catal., A 233 (2002) 215-226. https://doi.org/10.1016/S0926-860X(02)00147-3

[11] J.J. Spivey, K.M. Dooley, Catalysis (RSC Publishing) 19 (2006) 1. https://doi.org/10.1039/9781847555229-00001

[12] L. Guczi, G. Stefler, Z. Koppany, L. Borko, React. Kinet. Catal. Lett. 74 (2001) 259. https://doi.org/10.1023/A:1017933027153

[13] A. Feller, M. Clayes, E. van Steen, J. Catal. 185 (1999) 120. https://doi.org/10.1006/jcat.1999.2497

[14] G. Kiss, C.E. Kliewer, G.J. DeMartin, C.C. Culross, J.E. Baumgartner, J. Catal. 217 (2003) 127. https://doi.org/10.1016/S0021-9517(03)00054-X

[15] M.K. Gnanamani, G. Jacobs, U.M. Graham, W.P. Ma, V.R.R. Pendyala, M. Ribeiro, B.H. Davis, Catal. Lett. 134 (2010) 37. https://doi.org/10.1007/s10562-009-0213-7

[16] A.Y. Khodakov, A. Griboval-Constant, R. Bechara, V.L. Zholobenko, J. Catal. 206 (2002) 230. https://doi.org/10.1006/jcat.2001.3496

[17] X.L. Pan, X.H. Bao, Chem. Comm. 47 (2008) 6271. https://doi.org/10.1039/B810994J

[18] K.P. De Jong, J.W. Geus, Catal. Rev. 42 (2000) 481. https://doi.org/10.1081/CR-100101954

[19] Q. Zhang, J. Kang, Y. Wang, ChemCatChem 2 (2010) 1030. https://doi.org/10.1002/cctc.201000071

[20] J.F. Shackelford, W. Alexander, CRC Materials Science and Engineering Handbook, Third ed., CRC Press, Boca Raton, Florida, 2001, p. 404.

[21] P. Nguyen, C. Pham, Appl. Catal., A 391 (2011) 443. https://doi.org/10.1016/j.apcata.2010.07.054

[22] M. Lacroix, L. Dreibine, B. de Tymowski, F. Vigneron, D. Edouard, D. Begin, P. Nguyen, C. Pham, S. Savin-Poncet, F. Luck, M.J. Ledoux, C. Pharn-Huu, Appl. Catal., A 397 (2011) 62. https://doi.org/10.1016/j.apcata.2011.02.012

[23] Y.F. Liu, B. de Tymowski, F. Vigneron, I. Florea, O. Ersen, C. Meny, P. Nguyen, C. Pham, F. Luck, P.H. Cuong, ACS Catal. 3 (2013) 393. https://doi.org/10.1021/cs300729p

[24] A.R. de la Osa, A. De Lucas, A. Romero, J.L. Valverde, P. Sanchez, Catal. Today 176 (2011) 298. https://doi.org/10.1016/j.cattod.2010.12.010

[25] J.A. Diaz, M. Calvo-Serrano, D.R. de la Ana, A.M. Garcia-Minguillan, A. Romero, A. Giroir-Fendler, J.L. Valverde, Appl. Catal. A 475 (2014) 82. https://doi.org/10.1016/j.apcata.2014.01.021

[26] J. Labuschagne, R. Meyer, Z.H. Chonco, J.M. Botha, D.J. Moodley, Catal. Today 275 (2016) 2. https://doi.org/10.1016/j.cattod.2016.01.039

[27] A. Lillebo, S. Havik, E.A. Blekkan, A. Holmen, Top. Catal. 56 (2013) 730. https://doi.org/10.1007/s11244-013-0032-3

[28] Y.F. Liu, O. Ersen, C. Meny, F. Luck, P.H. Cuong, ChemSusChem 7 (2014) 1218. https://doi.org/10.1002/cssc.201300921

[29] S. Gryn, T. Nychyporuk, I. Bezverkhyy, D. Korytko, V. Iablokov, V. Lysenko, S. Alekseev, ACS Appl. Nano Mater. 1 (2018) 2609. https://doi.org/10.1021/acsanm.8b00301

[30] V. Iablokov, S.K. Beaumont, S. Alayoglu, V.V. Pushkarev, C. Specht, J.H. Gao, A.P. Alivisatos, N. Kruse, G.A. Somorjai, Nano Lett. 12 (2012) 3091. https://doi.org/10.1021/nl300973b

[31] S.A. Alekseev, V.N. Zaitsev, J. Botsoa, D. Barbier, Chem. Mater. 19 (2007) 2189-2194. https://doi.org/10.1021/cm0629107

[32] S. Alekseev, D. Korytko, M. Iazykov, S. Khainakov, V. Lysenko, J. Phys. Chem. C 119 (2015) 20503. https://doi.org/10.1021/acs.jpcc.5b06524

[33] Y. Han, S.S. Lee, J.Y. Ying, Chem. Mater. 19 (2007) 2292. https://doi.org/10.1021/cm063050x

[34] J. Schweicher, A. Bundhoo, A. Frennet, N. Kruse, Catal. Lett. 144 (2014) 204. https://doi.org/10.1007/s10562-013-1161-9

[35] G.L. Bezemer, J.H. Bitter, H.P.C.E. Kuipers, H. Oosterbeek, J.E. Holewijn, X. Xu, F. Kapteijn, A.J. van Dillen, K.P. de Jong, J. Am. Chem. Soc. 128 (2006) 3956. https://doi.org/10.1021/ja058282w

[36] D.B. Bukur, Z. Pan, W. Ma, G. Jacobs, B.H. Davis, Catal. Lett. 142 (2012) 1382. https://doi.org/10.1007/s10562-012-0908-z

[37] W. Ma, G. Jacobs, Y. Ji, T. Bhatelia, D.B. Bukur, S. Khalid, B.H. Davis, Top. Catal. 54 (2011) 757. https://doi.org/10.1007/s11244-011-9699-5

[38] G. Jacobs, T.K. Das, Y. Zhang, J. Li, G. Racoillet, B.H. Davis, Appl. Catal., A 233 (2002) 263. https://doi.org/10.1016/S0926-860X(02)00195-3

[39] R.C. Reuel, C.H. Bartholomew, J. Catal. 85 (1984) 78. https://doi.org/10.1016/0021-9517(84)90111-8

[40] L. Wei, Y. Zhao, Y. Zhang, C. Liu, J. Hong, H. Xiong, J. Li, J. Catal. 340 (2016) 205-218. https://doi.org/10.1016/j.jcat.2016.04.019

[41] M. Athariboroujeny, A. Raub, V. Iablokov, S. Chenakin, L. Kovarik, N. Kruse, ACS Catal. 9 (2019) 5603. https://doi.org/10.1021/acscatal.9b00967

[42] M. Cargnello, C. Chen, B.T. Diroll, V.V.T. Doan-Nguyen, R.J. Gorte, C.B. Murray, J. Am. Chem. Soc. 137 (2015) 6906. https://doi.org/10.1021/jacs.5b03333

[43] J. Y. Park, C. Aliaga, J.R. Renzas, H. Lee, G.A. Somorjai, Catal. Lett. 129 (2009) 1. https://doi.org/10.1007/s10562-009-9871-8

[44] B. Todic, W. Ma, G. Jacobs, N. Nikacevic, B.H. Davis, D.B. Bukur, Int. J. Chem. Kinet. 49 (2017) 589. https://doi.org/10.1002/kin.21133

[45] R.J. Madon, E. Iglesia, S.C. Reyes, in: M.E. Davis, S.L. Suib (Eds.), Selectivity in Catalysis, ACS Symposium Series, 517, 1993, p. 383.

[46] H. Karaca, J. Hong, P. Fongarland, P. Roussel, A. Griboval-Constant, M. Lacroix, K. Hortmann, O.V. Safonova, A.Y. Khodakov, ChemComm. 46 (2010) 788. https://doi.org/10.1039/B920110F

[47] P. Munnik, P.E. de Jongh, K.P. de Jong, J. Am. Chem. Soc. 136 (2014) 7333. https://doi.org/10.1021/ja500436y

[48] J.R.A. Sietsma, J.P. den Breejen, P.E. de Jongh, A.J. van Dillen, J.H. Bitter, K.P. de Jong, Stud. Surf. Sci. Catal. 167 (2007) 55. https://doi.org/10.1016/S0167-2991(07)80108-X

[49] D. Kistamurthy, A.M. Saib, D.J. Moodley, J.W. Niemantsverdriet, C.J. Weststrate, J. Catal. 328 (2015) 123. https://doi.org/10.1016/j.jcat.2015.02.017

[50] J. van de Loosdrecht, I.M. Ciobica, P. Gibson, N.S. Govender, D.J. Moodley, A.M. Saib, C.J. Weststrate, J.W. Niemantsverdriet, ACS Catal. 6 (2016) 3840. https://doi.org/10.1021/acscatal.6b00595

[51] J. van de Loosdrecht, M.D.J.L. Visagie, Top. Catal. 57 (2014) 430. https://doi.org/10.1007/s11244-013-0198-8

[52] I.G. Solomonik, K.O. Gryaznov, V.F. Skoka, V.Z. Mordkovich, RSC Adv. 5 (2015) 78586. https://doi.org/10.1039/C5RA11853K